Temperature dependence of the exchange stiffness in FePd(001) thin films: Deviation from the empirical law $A(T) \propto M_S^2$ at intermediate temperatures

M. Mulazzi,[1] A. Chainani,[2,3] Y. Takata,[2,3] Y. Tanaka,[2,3] Y. Nishino,[2] K. Tamasaku,[2] T. Ishikawa,[2] T. Takeuchi,[2] Y. Ishida,[3] Y. Senba,[4] H. Ohashi,[4] and S. Shin[1,3]

[1]*The University of Tokyo, Institute of Solid State Physics, 227-8587 5-1-5 Kashiwanoha, Kashiwa, Japan*

[2]*Coherent X-ray Optics Group, RIKEN SPring-8 Centre, Sayo-cho, Hyogo, 679-5148, Japan*

[3]*Excitation Order Research Team, RIKEN SPring-8 Centre, Sayo-cho, Hyogo, Japan*

[4]*JASRI/SPring-8, Sayo-cho, Hyogo, 679-5198, Japan*

(Received 12 December 2007; revised manuscript received 16 May 2008; published 16 June 2008)

We study the temperature dependence of the exchange stiffness $A(T)$ of a thin FePd(001) film, which exhibits well-ordered magnetic stripe domains. We employed two different methods: (i) applying an exact micromagnetic model of the nucleation point and (ii) a detailed analysis of the temperature dependence of the saturation magnetization. The experimental data needed as input for the theoretical model are the stripe domain width and the nucleation field, and these were obtained as a function of temperature using soft x-ray magnetic scattering and superconducting quantum interference device (SQUID) magnetometry, respectively. The temperature independence of the domain width is very important from the point of view of the energetics of the FePd film, i.e., the number of magnetic domains remains constant per unit area. From this experimental finding we infer that the exchange stiffness must vary as a function of the temperature. We show that the $A(T)$ dependence obtained with the two procedures are consistent but different from the phenomenological law $A(T) \propto M_S^2(T)$, normally assumed to be valid in the temperature range examined ($T=50-250$ K), an intermediate temperature range for which there is no known expression of the magnetization as a function of the temperature. We have also investigated the Fe 3*s* core level and valence band of FePd using hard x-ray photoemission spectroscopy. The Fe 3*s* spectra exhibit negligible changes in the temperature range investigated, while small changes occurring over large energy scales are observed in the valence-band spectra. Based on the lack of consistency of the magnetometry and scattering results compared to local-moment theories, these results favor an itinerant magnetism picture for FePd.

DOI: 10.1103/PhysRevB.77.224425 PACS number(s): 75.20.En, 75.30.Et, 75.60.−d, 78.70.Ck

I. INTRODUCTION

In the last 20 years the miniaturization of electronic devices has led to the development of memory bits (=unit information carriers) of the size of tens of nanometers. It was also realized that besides the proportional increase in the computing power, nanostructured matter shows new phenomena originating in its quantum nature. The quantum Hall effect and the giant magnetoresistance are typical examples of how the reduced dimensionality reveals new physics. In the field of magnetic memories, the race for ultrahigh data storage media has been driven by the concept of finding materials with high perpendicular magnetocrystalline anisotropy (PMA), i.e., materials in which the magnetization vector would be naturally oriented perpendicular to the sample surface. The higher the PMA, the smaller would be the lateral size of the information-carrying unit at room temperature without encountering the so-called "superparamagnetic limit."

FePd films are well known to exhibit magnetic stripe domains with a Curie temperature $T_C=713$ K. The FePd alloy has been regarded as a candidate for high magnetic data storage for its very high PMA that can be achieved in a rather simple way, i.e., controlling the substrate temperature during the growth.[1,2] In addition to the PMA, other parameters considered important for designing a device for data storage are: the exchange stiffness A, the saturation magnetization M_S, and the remanence field. All of them are important to determine its behavior for the "up-to-down" switching magnetic field and the minimum thickness required of a thin film for memory applications, before the demagnetization energy overcomes the PMA. Among the above-mentioned parameters, the exchange stiffness A is one of the experimentally less-studied properties of a ferromagnet. The exchange stiffness A is directly proportional to the magnetization per unit volume,[3] it determines the thickness of the Bloch wall, as well as the decrease in saturation moment with increasing temperature in a ferromagnet. However, it is intrinsically difficult to measure, and reliable values can be obtained only from measurements of the saturation magnetization at low temperatures or from the spin-wave frequency determined from ferromagnetic resonance experiments. Cruder estimates can be done using the Curie temperature and the spin magnetic moment. Nonetheless, the very low-temperature regime has been well-studied by several groups, which confirm that the magnetization follows the theoretically predicted Bloch law,[4]

$$M_S(T) \propto T^{3/2}. \tag{1}$$

On the other hand, just below T_C, the magnetization is expected to follow a power law with

$$M_S(T) \propto (T_C - T)^{\beta}, \tag{2}$$

where β is a critical exponent and its value depends on a specific model based on local spins, typically, the Ising or

Heisenberg models. At intermediate regimes, neither behavior holds because the low-temperature spin-wave dominated magnetization dynamics and the high-temperature nonadiabatic localized fluctuations mix up. However, below T_C, A has been reported to follow

$$A(T) \propto M_S(T)^2, \tag{3}$$

derived from qualitative arguments.[5] While A must go to zero when ferromagnetism disappears at the Curie point, the above-mentioned phenomenological law has been recently confirmed for FePd in the high-temperature regime below T_C ($300 < T < 700$ K).[6] Investigations in the intermediate regime can hopefully give insights into the mechanisms of the crossing over from one regime to the other, and this is the focus of the present study. In this work, we investigate the temperature dependence of A at intermediate temperatures (50–250 K), using two different sets of experimental data [soft x-ray magnetic scattering and superconducting quantum interference device (SQUID) magnetometry] and an exact micromagnetic model of nucleation. We find consistent behavior of the exchange stiffness as a function of temperature between 50–250 K, but the data show deviations from the phenomenological $A(T) \propto M_S(T)^2$.

We also discuss the observed behavior of the density of states (DOS), on the basis of complementary hard x-ray photoemission spectroscopy (HXPES) of the valence band and known spin-resolved band-structure calculations.

II. EXPERIMENT RESULTS

The sample we examined is a 45-nm-thick FePd equiatomic alloy grown using layer-by-layer molecular beam epitaxy (MBE) on an MgO(001) substrate. A chromium seed of 2 nm was grown on the MgO and a subsequent 600 nm palladium buffer layer was deposited to reduce the lattice parameter mismatch before growing the FePd film. Finally, a pure palladium 2-nm-thick capping layer was grown to prevent oxidation of the FePd film. The value of the quality factor $Q = 2K_u/\mu_0 M_S$ determined by vibrating sample magnetometry (VSM) is about 0.4, obtained using a value of 1030 emu/cm^3 for the saturation magnetization and is indicative of weak PMA.

The exchange stiffness $A(T)$ has been determined from two different methods: (i) by measuring the saturation magnetization $M_S(T)$ and (ii) measuring the stripe domain width and the nucleation field as a function of the temperature and applying an exact model of the nucleation process. In order to measure $M_S(T)$ and domain nucleation field we used SQUID magnetometry in the 5–330 K range, while the domain width W was measured with magnetic force microscopy (MFM) (at room temperature) and soft x-ray magnetic scattering (SXRMS) from 50–250 K. The magnetization curve is presented in Fig. 1.

It shows the normalized magnetic moment per unit volume (calculated using the nominal growth value for the thickness). This curve was measured applying a $H = 6$ kG field in order to saturate the in-plane magnetization. A contribution from nonmagnetic impurities has been subtracted using a Curie–Weiss law in the low-temperature region. The

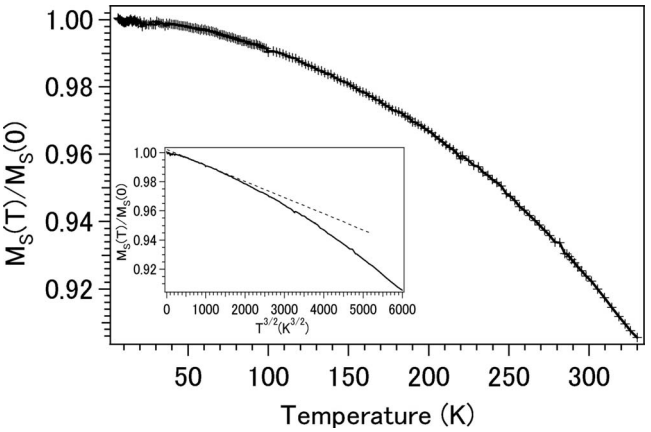

FIG. 1. Saturation magnetization as a function of the temperature measured by a SQUID magnetometry. The data have been normalized to the magnetization at the absolute zero, $M_S(0) = 1013$ emu/cm^3. In the inset the reduced magnetization is plotted versus $T^{3/2}$; a guide to the eye dashed line simulates the Bloch law for a constant exchange stiffness and the deviation from the experimental data in the intermediate temperature regime.

saturation magnetization at the absolute zero obtained from the data of Fig. 2 is 1013 emu/cm^3, which is consistent with the one obtained by VSM.

Hysteresis cycles have been determined using magnetic fields ranging from -3–3 kG applied parallel to the surface plane. Since the sample was a thin film with PMA, the relative alignment of the sample and the field direction is very important and has been checked carefully. Moreover, in order to avoid artifacts the hysteresis cycles and the field cooling curve has been measured within the same experiment, i.e., without removing and remounting the sample in the experimental apparatus. The diamagnetic contribution of the MgO substrate has been removed by means of a linear fit of the high magnetic field data ($1 \leq H \leq 3$ kG and $-3 \leq H \leq -1$ kG). The contribution of the paramagnetism of the Pd buffer layer is implicitly removed together with the MgO diamagnetism.

In the top part of Fig. 2 four hysteresis cycles at four different temperatures, 100, 150, 200, and 250 K, are shown.

At the highest magnetic field shown, it is possible to see that the saturation magnetization decreases with the temperature, consistently with the data of Fig. 1. The other features of the cycles, the remanent magnetization and the coercive field, are not modified by the temperature. However, the nucleation field, i.e., the magnetic field at which the magnetic domains appear out of the saturation condition, varies from 1.7 (at 100 K) to 1.3 kG (at 250K) as seen in the inset of Fig. 2.

The magnetization distribution at room temperature was imaged by a MFM in air using a CoCr alloy tip and after applying and removing an in-plane field of a 5000 G to magnetize the sample. Figure 3 shows the MFM image measured on a very wide scale, 8×4 μm^2.

As seen in the image, the long-range order is excellent over a wide scale, despite the presence of structural defects, i.e., the white dots and the "canyons." They were also recorded in the topographical atomic force microscopy (AFM)

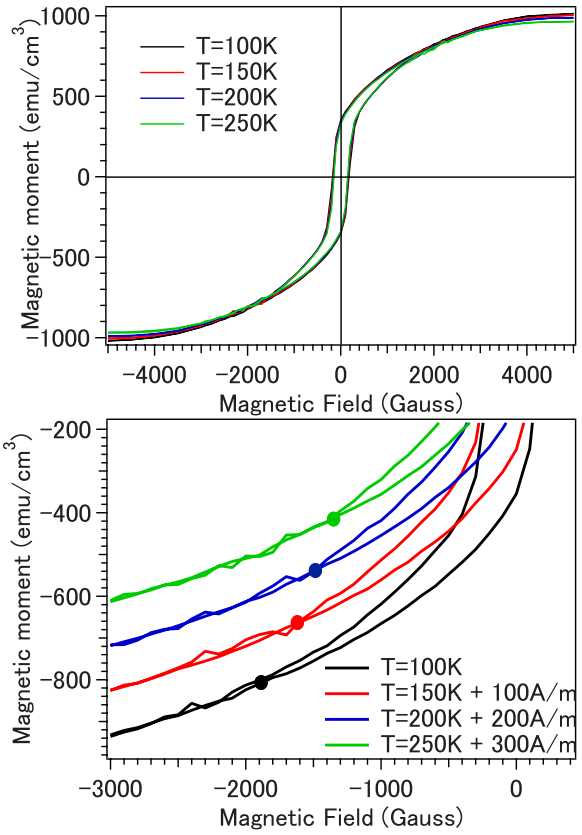

FIG. 2. (Color online) In the top panel, four hysteresis cycles are shown, after correcting for the MgO substrate diamagnetism. Although looking quite similar, clear differences can be found in the value of the saturation magnetization at the different temperatures. In the bottom panel, a zoom of the hysteresis cycles in the region of the nucleation point is shown. The nucleation point is shown by a filled dot and it changes as a function of the temperature. An artificial offset, as indicated in the label, has been added to each curve for clarity.

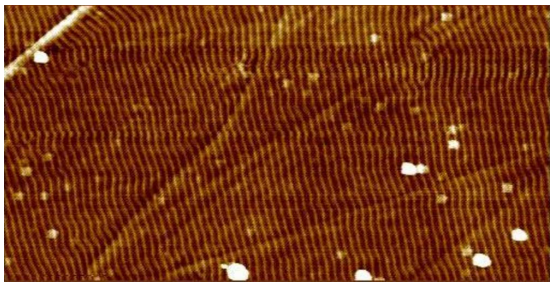

FIG. 3. (Color online) MFM image of the FePd thin film measured in air, the image is 8×4 μm^2. The yellow and brown stripes can be identified as the magnetic domains. From the size of the image it is possible to see that the domains are well ordered beside the surface roughness and the topological defects (white spots). From a line profile of this image, we were able to measure the lateral resolution to be 30 nm, roughly as wide as the cantilever tip. This does not forbid a clear determination of the domain width as the distance between two adjacent maxima or minima of the intensity.

image (not shown) measured together with the MFM one. From the data of Fig. 3, we get a domain width of 50 ± 3 nm. The MFM image gave another important information: the stripe domain pattern is homogeneous up to a scale comparable to the size of synchrotron radiation beam (10×10 μm) available at the beamline BL17SU where the scattering experiments have been carried out. Thus the information determined by the scattering experiments can be considered as intrinsic, i.e., derived from a well-ordered stripe domain pattern and not an average over a disordered state.

SXRMS has been used to measure the temperature dependence of the domain width since the MFM could operate only in air at room temperature. SXRMS is a photon-in–photon-out technique probing the magnetic ordering through a contribution to the scattering factors proportional to the magnetization.[7–9] This contribution becomes measurable when the photon energy is tuned to an absorption edge of an atom carrying a magnetic moment (either spontaneous or induced). Because of the resonant intensity enhancement, magnetic scattering has become a popular technique at synchrotron radiation sources where high-resolution brilliant beams are available. As any diffractive technique, magnetic scattering is sensitive to long-range order, thus the signal is appreciable only on samples with well-ordered magnetic lattices. The stripe domains of FePd constitute a magnetic lattice that can give rise to magnetic Bragg peaks whose position in the reciprocal space is directly related to the magnetic domain width W ,[6,10–12] $W=2\pi/q_x$.

The experiments have been carried out at the BL17SU beamline of the SPring-8 synchrotron radiation facility using a diffractometer, which allows regular θ-2θ scans, as well as azimuthal and tilting rotation for optimum crystal alignment. The beam is delivered by a helical undulator, which covers the $400\leq h\nu\leq2000$ eV energy range. The high stability of the beam energy (±5 meV at $h\nu=708$ eV, the iron L_3 resonance energy) and the high angular resolution ($\Delta\theta=0.01°$) make the determination of the magnetic domain width and coherence length effectively independent of the instrumental uncertainites.

The thermal stability of the samples was checked from the experiments by measuring the magnetic scattering peaks in a temperature cycle, and the results were confirmed to be reproducible. Similarly, the magnetometry results discussed earlier and the photoemission results in the following were also confirmed to be reproducible.

Despite the lack of a polarization analyzing crystal to remove the charge scattering signal, the magnetic scattering peaks were clearly observed. In Fig. 4(a), an example of rocking curve allowing for the measurement of the photon intensity as a function of q_x, the component of the transferred momentum parallel to the surface, is shown.

Three main peaks appear: the one at $q_x=0$ Å^{-1} is the specular peak appearing when the incidence angle θ is exactly half of 2θ. At the sides of the specular peak the intensity does not decrease to zero because of the diffuse scattering induced by the surface defects and by the mosaicity of the crystal. The two small peaks appearing at a finite $|q_x|$ are the so-called magnetic satellite peaks. At even wider angles the intensity drops very fast because the total reflection limit has been reached (Yoneda angle). From the above-mentioned

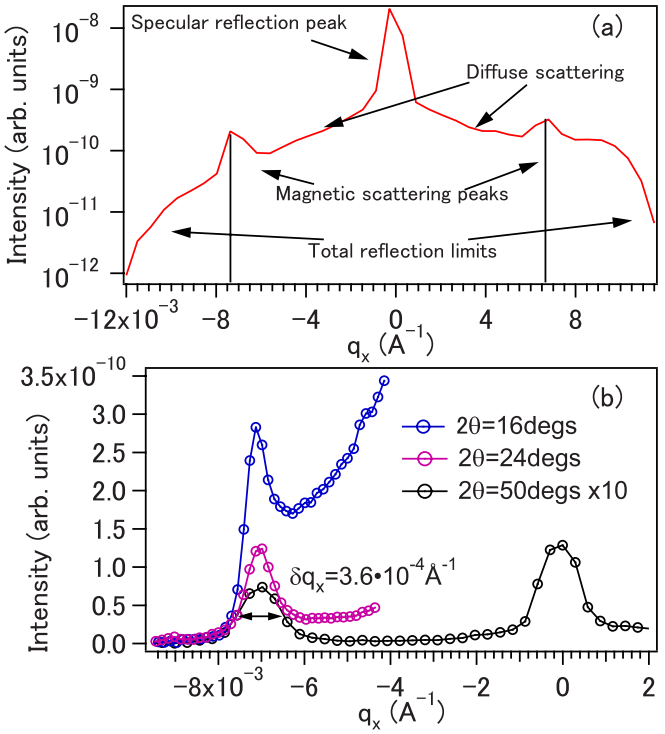

FIG. 4. (Color online) (a) Example of rocking curve measured to determine the stripe domain width at room temperature. The central specular peak, occurring when the incidence angle θ equals half of the detection angle 2θ, the diffuse scattering background, due to the surface imperfections, and at wider angles the magnetic scattering satellites giving the stripe domain are explained in the text. (b) The q_z dependence of one of the magnetic scattering peak: the peak position is constant, while the diffuse scattering is strongly reduced at high incidence angles. The data acquisition time of the curve at $2\theta=50°$ is the same as the other ones, but multiplied later by a factor of 10 so as to compare to the other two. We want to stress on the high quality of the experimental data: Even at $\theta=25°$ incidence angle the magnetic scattering peak is clearly observed and its intensity is comparable to the specular one. The noise is also very low, despite the smallness of the signal, ≈0.1 pA at the background level.

relation we infer that the domain width is $W=46\pm3$ nm, in good agreement with the value obtained by MFM. We stress on the fact that despite the high roughness of the surface (measured by MFM is about 10 nm, from the top of the highest white dot to the bottom of the deepest "canyon") it was possible to obtain clear magnetic scattering peaks. From Fig. 4(b) we can extract the coherence length of the magnetic domains, i.e., $\frac{\pi}{\Delta q_x}=8640$ Å ≈ 860 nm, roughly 190 domain widths.

Experimentally, the domain width has been measured both with the MFM and in the SXRMS experiments keeping the sample at remanence and not at the nucleation point. One could argue that the domain width could be different in the two situations, but this possibility was ruled out for FePd by a previous study.[6,12]

As seen in Fig. 5, the domain width is almost unchanged in the 50–200 K temperature range. An average value of $W=46$ nm has been derived from a linear fit of the data con-

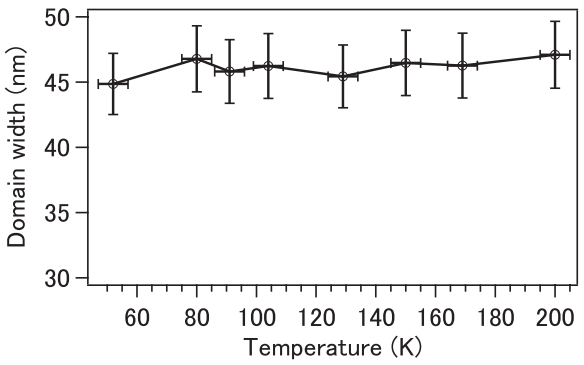

FIG. 5. Temperature dependence of the domain width as measured by SXMRS. As seen, W is temperature independent and the average domain width is $W=46\pm3$ nm.

sidering the error bars of every data point at the different temperatures. The lack of a temperature dependence of domain width has important implications for the energetics of the FePd thin film, as discussed later.

The HXPES data was collected at the beamline BL29U of SPring-8. The photon energy used was $h\nu=7939$ eV, high enough to achieve a ≈6 nm escape depth for the photoelectrons.[13] The analyzer was a VG Scienta R4000 featuring a ±20° angular acceptance operated in the angle-integrating mode because of the very high photon energy. The grazing incidence of the x-ray beam on the surface (incidence angle ≈0.3°) and the light polarization vector perpendicular to the surface plane enhance the photoemission along the normal emission direction, where the energy analyzer is located. With such an instrument, the photoelectron intensity may be as much as ≈100 times higher than in a wide incidence angle configuration,[14] thus reducing the average counting time to approximately ten minutes for a valence-band spectrum. The valence-band photoemission spectra collected at room temperature and at $T=50$ K are showed in Fig. 6.

They were acquired fixing the experimental resolution to 230 meV, mainly determined by a choice of the analyzer pass energy (PE=200 eV), as checked by measuring the width of the Fermi edge of a polycrystalline gold sample in electrical contact with the FePd film. The spectral line shape is very similar at both the temperatures, but we notice that in the mid of the d-band complex (−2.0 to −5 eV binding energy) the low-temperature data are slightly higher while the situation reverses near the Fermi level (0 to $-1.5E$ binding energy). These are the first experimental data on the valence band of a FePd thin film or single crystal. It has not been possible to find any other measurement of the FePd valence band in the literature. The comparison of our data to previous band-structure calculations[15–17] allows us to assign the various experimental peaks to the spin-resolved density of states of iron and of palladium. The shoulder close to the Fermi level is derived from Fe minority electrons, which constitute also the largest part of the DOS at the Fermi level. The large block of bands between −1.5 and −5.5 eV binding energy can be divided in three main contributions (at ≈−1.5 eV, ≈−2.5 eV, and ≈−3.5 eV) the first and the third of which can be attributed to mainly Fe majority spin while the second

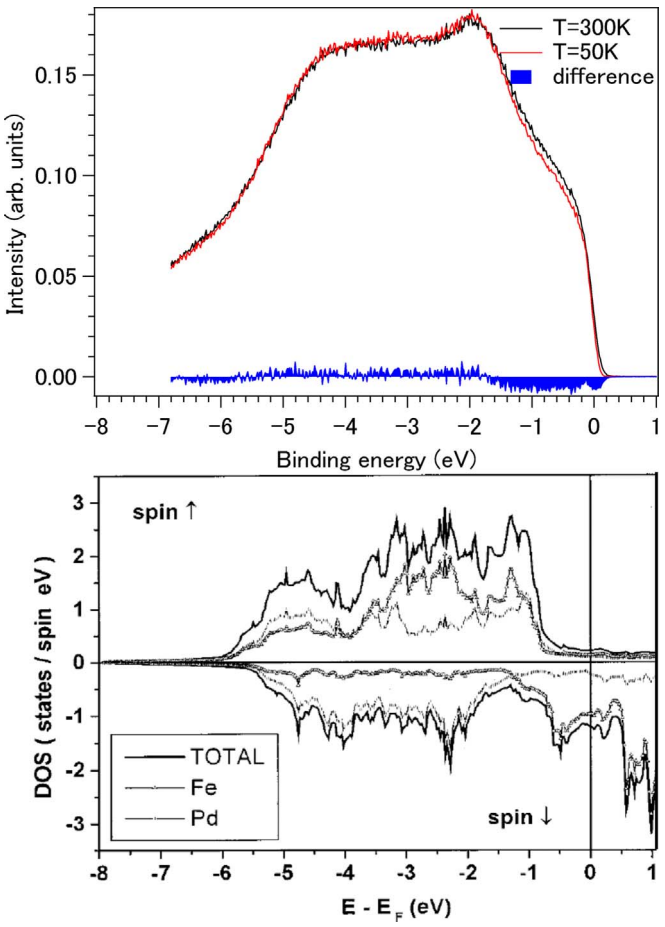

FIG. 6. (Color online) In the upper part we present the HXPES data taken at two different temperatures and referred to the Fermi level of a polycrystalline Au sample. As noticed FePd at room temperature has a higher DOS close to the Fermi level than at $T=50$ K, while in the d-band complex the situation reverses. From both the curves an integral background has been subtracted and both have been divided by their respective integral from +1 to −7.5 eV for a common normalization. The blue waterfall line at the bottom shows the difference between the two curves obtained after the normalization procedure described in the text was applied. The lower part, taken from Garcia *et al.* (Ref. 15), shows the spin-resolved DOS for an ordered FePd bulk calculated in the local spin density approximation for the magnetization vector aligned along the (100) axis.

one is consists of the Pd electronic states. The tail at higher binding energy is of majority Fe and Pd character mixed with equal weight.

The comparison between the HXPES data and theory needs some comment. The calculation shows the DOS inside the muffin-tin orbitals, mainly containing the localized d electrons while implicitly reducing the contributions of the more delocalized sp bands. On the other hand, the photoemission data are taken using very high energy photons that enhance the contributions of sp electron with respect to the d ones. However, despite this remark, we notice that the d bands normally form sharp peaks in the DOS, such as the ones we observe in the experiment, while the sp bands form a flatter and smaller "background." For this reason we are confident that the assignment of the peaks can be considered reliable even if the cross sections of the d electrons is reduced with respect to the sp ones.

It is noted that although the ratio between the calculated atomic photoemission cross sections of sp and d electrons becomes favorable to the former at high energy compared to UV or soft x-ray photoemission, recent HXPES experiments on $3d$ and $4d$ systems (such as vanadate,[18] cobaltate,[19] and silver metal[20]) show only small increase in the relative intensities of the sp states and the valence-band spectra are still dominated by d-electron states.

The data of Fig. 6 are presented after a normalization procedure has been applied: first an integral background is removed from each data set, then each curve is divided by the respective energy integral. This procedure brings the spectra taken at two different temperatures on the same (arbitrary) intensity scale and, more importantly, imposes the conservation of the total number of electrons. The energy integral of the difference curve should be equal to zero in the ideal case (exact conservation of the total number of electron), but for the data presented here it amounts to ≈0.1% of the intensity average of the two curves.

In Fig. 6 the difference of the two photoemission spectra measured at different temperatures shows a redistribution of the photoelectron intensities induced by the change of temperature on a very wide scale. This is a hint that a change in the electronic structure changes the magnetic state of FePd.

III. DOMAIN WIDTH AND NUCLEATION FIELD ANALYSIS WITH THE MICROMAGNETIC MODEL

The exchange stiffness has been accessed applying a model for the nucleation of stripe domains using the nucleation field and the magnetic diffraction data. This model was first introduced by Muller and Brown[21,22] and later described in more detail by Hubert and Schaefer,[23] who treated it analytically in the case of vanishingly small anisotropy. The exact numerical solution of the model and the application to the stripe domains of FePd in the high-temperature region was investigated by Asti *et al.*,[6] and we refer to that work for the detailed description of the model and to the subtleties of its solution. As for a short description, it is based on the static case of the Landau–Lifshitz equations of micromagnetism,[23–25] which were derived from the energy equilibrium condition for a ferromagnetic film with uniaxial PMA in a magnetic field oriented parallel to the surface plane. At the nucleation point the equations can be linearized and exact solutions can be derived using a "plane wave" Ansatz. Once these solutions are introduced in the differential equations, they lead to algebraic equations for the plane-wave amplitude that can be solved to give the phase diagram of the nucleation process.

We should stress here that no approximation has been used in the solution of the model, except considering that at nucleation the magnetization components perpendicular to the field are small. The lack of a surface and quartic anisotropy terms may be regarded as implicit approximations, but we should note that for the FePd film under investigation the second-order anisotropy term is small, $Q=0.4$, thus the quar-

tic term can be considered even smaller. Moreover, since the hysteresis cycles are always monotonic from zero field to saturation, we think the quartic contribution can be safely neglected. The surface anisotropy term is important for ultrathin films, whose thicknesses are usually smaller than 10 monolayers, and it decreases with the inverse of the thickness. Thus, we consider also the surface energy term as negligible for our FePd film.

The model needs; as inputs, the sample thickness, the domain width, the saturation magnetization, and the nucleation field H_C; and as output, the anisotropy constant and the exchange stiffness. Using the different values for W and H_C obtained at the different temperatures, we obtained the values for the exchange stiffness summarized in Fig. 8. As a micromagnetic model, it does not contain the temperature explicitly, but the solutions to the model equations have to be considered as relationships between parameters all evaluated at the same temperature.

From a linear fit of the data and an extrapolation at $T=0$ K, we obtain the value of $A(0)=9.1\times10^{-11}$ J/m, which is a typical value for a transition metal ferromagnet. We notice however that,

$$R_{\text{model}} = 1 - \frac{A_{\text{model}}(250)}{A_{\text{model}}(0)} \approx 0.18,$$

while we extract from the saturation magnetization data, the experimental value of

$$R_{\text{mag}} = 1 - \frac{A_{\text{mag}}(250)}{A_{\text{mag}}(0)} = 1 - \left[\frac{M_S(250)}{M_S(0)}\right]^2 \approx 0.09,$$

which is a half of what we have obtained from the micromagnetic model, using the experimentally determined domain width and nucleation field. This means that the measured $A(T)$ decrease is stronger than expected. In order to check the consistency of the result, we analyze the saturation magnetization as a function of the temperature in the following section.

IV. ANALYSIS OF $M_S(T)$

It is well known that the saturation magnetization decreases following the Bloch law at low temperatures because of the thermal excitation of magnons. The analysis of the field cooling data starts with a fit to the formula,

$$\frac{M_S(T)}{M_S(0)} = 1 - \alpha T^{3/2},$$

in three cases: (i) the $5 \le T \le 90$ K region, (ii) the whole temperature region forcing $M_S(0)=1$, and (iii) the whole region without any fixed parameter.

As seen in Fig. 7 all the three cases give unsatisfactory results over the full temperature range, while the best result is obtained if the temperature is restricted to below 90 K [case (i)]. Even for this case, just outside the fitting range at about 100 K, the experimental data deviate from the theory, which is a sign that phenomena other than magnon excitations are becoming relevant. Deviations from the Bloch law are known to happen because of magnon-magnon scattering,[27] but it was also suggested[28,29] that a temperature variation of the exchange constant may explain the thermal behavior of the saturation magnetization of ferromagnets. We notice that the temperature dependence of the saturation magnetization contains implicitly the temperature dependence of the exchange stiffness $A(T)$ through the following formula:[30]

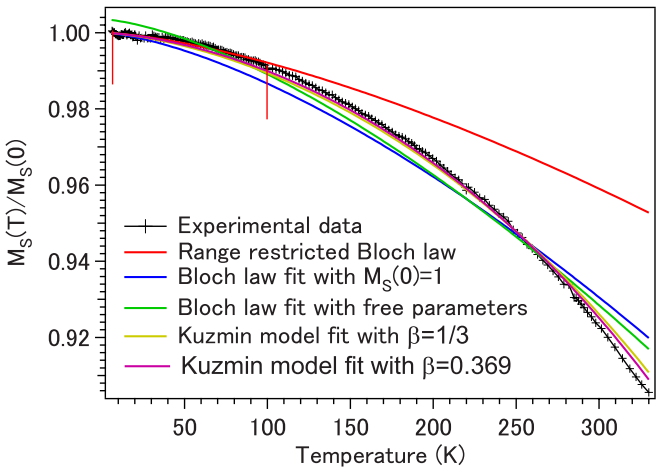

FIG. 7. (Color online) Fits of the reduced magnetization data (black line and crosses) of Fig. 1 using different model functions and choice of ranges and parameters: (red) Bloch law at low-T region only (range delimited by the red vertical bars), (blue) Bloch law for the whole data set and $M_S(0)=1$, and (green) whole data set and all the parameters left free to vary; (ochre) Kuz'min (Ref. 26) formula with $\beta=1/3$ (with $s=0.499\pm0.005$) and (purple) $\beta=0.369$ (with $s=0.404\pm0.004$). For the last two fits the reduced magnetization at $T=0$ K has been forced to one, the Curie temperature fixed to be $T_C=690$ K[4], and $p=5/2$. A significant improvement of the χ^2 of the fit can be obtained leaving the Curie temperature free to vary, but a value of $T_C=620$ K is obtained. Such a value is unphysical since clear magnetic peaks could be obtained at higher temperatures and the result of the fit with free parameters must be rejected.

$$\frac{M_S(T)}{M_S(0)} = 1 - 0.0587\sqrt{Qs}\left[\frac{k_B T}{2A(T)a}\right]^{3/2}, \tag{4}$$

where Q is the number of nearest-neighbor atoms, a is the lattice parameter, k_B is the Boltzmann constant, and s is the spin quantum number.

$$s = \frac{M_S(0)a^3}{Qg\mu_B},$$

where g is the Landé factor and μ_B is the Bohr magneton. These formulas are obtained from the "classical" expression of the Bloch law involving the spin-wave stiffness D by noting that[31]

$$A = \frac{D\rho s}{2g\mu_B}. \tag{5}$$

Inserting the value of α obtained from the first fit and using the above-mentioned formulas, we obtain $A(0)=1.12\times10^{-11}$ J/m and $s=2.9$ using $g=2$. This value of g might

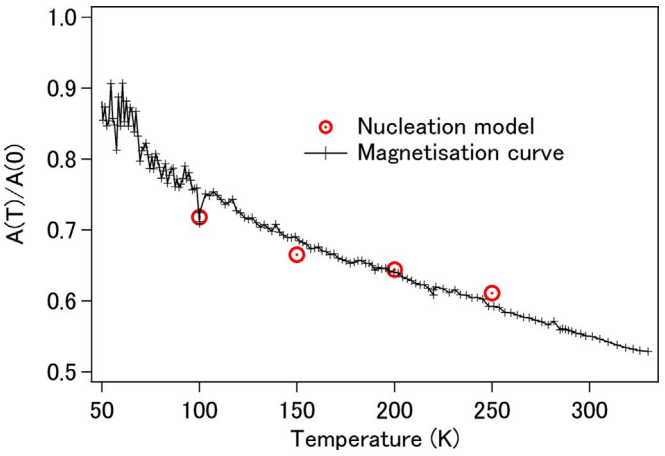

FIG. 8. (Color online) Comparison between the exchange stiffness temperature dependence obtained by the two methods described in the text.

not be correct but we had to use it since no value for FePd is available in the literature. We notice anyway that the dependence of A and s on g is rather small for small variations of g. The exchange stiffness at $T=0$ K obtained by the field cooling data compares quite well with that obtained by the micromagnetic model analysis. Since the temperature independence of the exchange stiffness is unphysical, we make the hypothesis that deviations from the Bloch law on increasing temperature originate from a temperature-dependent exchange stiffness. In order to extract $A(T)$ from the field cooling curve, we inverted Eq. (4) to obtain the following formula:

$$\frac{A(T)}{A(0)} = T\left[1 - \frac{M_S(T)}{M_S(0)}\right]^{-2/3} \tag{6}$$

Figure 8 plots the data obtained from the Eq. (6) together with those obtained by using the micromagnetic model.

The agreement between the two sets of data is noticeable, although only four values of the nucleation field could be measured. As previously suggested, the deviation from the empirical rule $A(T) \propto M_S^2$ is confirmed in the temperature range explored.

We have also carried out an analysis using a recent formula from Kuz'min[26,32] for the saturation magnetization, which is proposed to be valid for any kind of magnet from the absolute zero to the Curie temperature;

$$m(\tau) = [1 - s\tau^{3/2} - (1-s)\tau^p]^\beta, \tag{7}$$

where $\tau = T/T_C$, s is a free fitting parameter and $p = \frac{5}{2}$ for most of the materials investigated,[26] except for iron for which $p=4$. The β exponent can take values 1/3 or 0.369 depending on the universality class of the magnetic phase transition. In the proposed formula, the fitting parameters can be calculated from the first-principles but a specific microscopic model has to be chosen.

We see that in Eq. (7) the exchange stiffness does not appear, thus it is considered implicitly constant. The result of the fit to our saturation magnetization data is shown in Fig. 7. Two important points are to be noticed from the fitting results: (1) the choice of the critical exponent is irrelevant and (2) the results of the Kuz'min model are similar to the fits obtained with the Bloch law imposing $M_S(0)=1$. The reason for point (1) is simply that the data range ends too far from the Curie temperature and is not sensitive to it. Trying to explain point (2), we notice that there is an improvement in the result of the fit, the theoretical curve of Eq. (7) agrees better with the experiment than the fit with Eq. (4), but the qualitative behavior is the same. For this reason, we believe the introduction of a temperature-dependent exchange stiffness should improve the fit and possess a behavior similar, though flatter, to that of Fig. 8. We thus conclude that the $A(T) \approx M_S(T)^2$ relation does not hold even if an improved expression for the saturation magnetization temperature dependence is selected.

V. DISCUSSION

As already stated, the constant A approximation cannot hold on the general principle that the ferromagnetism has to disappear at the Curie point. On the other hand, at low temperature, one may argue that the critical temperature is so far that A can be considered constant. According to our data it is not so. Arguing qualitatively, since W is constant, as seen by SXRMS, the number of domains and of domain walls per unit volume does not change as a function of the temperature. From the point of view of energy balance, the different energy contributions, namely, exchange energy, demagnetization energy, anisotropy energy, and Zeeman energy must be at equilibrium at every temperature in order to keep the domain width constant. As observed, the saturation magnetization and the nucleation field decrease as a function of the temperature, thus decreasing the demagnetization and Zeeman energy contributions. Thus, also the exchange stiffness and the anisotropy K_u have to decrease accordingly. By this argument, one can justify a thermal variation of $A(T)$ in the low-temperature region even if no guess can be made on the actual mathematical form of the law.

We can also justify qualitatively the discrepancy between the behavior of $A(T)$ found and the phenomenological rule employed at low temperature. If Eq. (3) and Eq. (4) hold at the same time,

$$\begin{cases} M_S(T) = M_S(0)\left[1 - \alpha\left(\dfrac{T}{A(T)}\right)^{3/2}\right], \\ A(T) = \beta M_S(T)^2 \end{cases} \tag{8}$$

in which α and β are positive proportionality constants. If solved, Eq. (8) would give monotonically increasing functions for both $M_S(T)$ and $A(T)$ as a function of the temperature. Since this is unphysical, the dependence on $M_S^2(T)$ has to be abandoned because the Bloch law has been successfully verified in a wide variety of systems. The phenomenological rule can hold in other temperature regions in which the Bloch law does not hold strictly anymore, i.e., closer to the Curie temperature.

According to our analysis the Bloch $T^{3/2}$ law can be considered valid in the whole range of temperatures explored, but additionally the temperature dependence of the exchange

stiffness must be taken into account. From the microscopic point of view, the validity of the Bloch law implies that the quantum mechanical treatment of the magnons can be applied up to rather high temperatures $T \approx 330$ K $\approx 0.47 T_C$ and that up to this point magnon-magnon interaction can be neglected. On the other hand, the variation of the exchange stiffness implies that, according to Eq. (5), the spin-wave stiffness D may have a temperature dependence.

The HXPES data are a direct measure of the FePd DOS at two different temperatures whose difference is small and located at the Fermi level, which is populated by mainly iron minority spin electrons. HXPES is a genuine probe of the microscopic interactions giving rise to the electronic structure and magnetism. For this reason, a microscopic theory has to be used to interpret it. The macroscopic theory of magnetism can be classified in two wide categories according to the treatment of valence electrons,[33,34] i.e., localized or itinerant in the real space. As a rule of the thumb, transition metal oxides and rare-earth compounds are localized ferromagnets, while 3*d*-electron metals are itinerant ferromagnets. In the first case the Heisenberg model or its generalizations can be applied quite successfully, while for the second case there is no unified theory available to explain the temperature dependence of the magnetization.

To know which of the two models can be applied to FePd at low temperature, we note that the Heisenberg model gives a relationship between the exchange stiffness, the Heisenberg exchange integral and the spin magnetic moment. Such a relation and its derivation can be found in the Appendix as Eq. (A1), which is complementary to Eq. (5) when the relationship between the exchange integral and the magnon stiffness is known explicitly.[35] In both cases, a dependence on the squared saturation magnetization is evident, but is not supported by the experimental findings as discussed above. Thus we rule out the localized picture for the magnetism of FePd thin films at high temperature.

Turning to itinerant electron theories we notice that they are all based on the hypothesis that a net magnetic moment can only appear if a part of the majority (or minority) band is empty, i.e., there is an energy *exchange splitting* ΔE_{ex} between the two bands. This was already noticed in the HXPES data, which are consistent with spin-resolved band-structure calculations. However ΔE_{ex} must have a temperature dependence and it should become zero at the Curie point. Direct photoemission measurements have been reported since the 1970s for transition metal ferromagnets showing the thermal decrease in the exchange splitting.[36]

In our case it is not possible to identify directly the exchange splitting from the data of Fig. 9 because the maximum of the minority band lies too far in the empty states, as suggested by theoretical calculations.[15–17] We cannot also rule out a contribution of indirect transitions to the line shape, thus masking the magnetic effects.

In order to get some insight into the role of the minority electron states at the Fermi level, we divided the data of Fig. 6 by the Fermi–Dirac function broadened by the finite temperature and instrumental resolution and plotted them in Fig. 9. It is seen that the division by the Fermi–Dirac function only affects a ≈ 0.3 eV wide slice of the spectrum. The main effect is to evidence a small bump (another feature of the minority spin band) and to "create" a dip at $E_B \approx 0.2$ eV. However, it is possible to see that the intensity in the room-temperature curve is always higher than in the low-temperature ones.

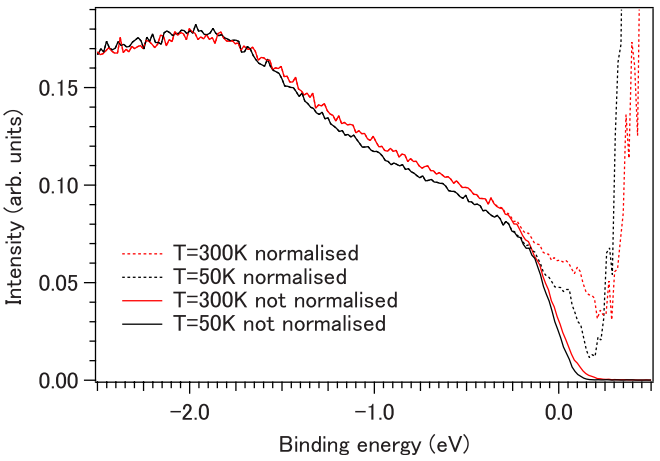

FIG. 9. (Color online) Zoom at the Fermi level of the HXPES data. The solid curves represent the data divided by the Fermi–Dirac function, while the dashed ones report the data before the division. Such procedure shows that the intensity up to ≈1.5 eV binding energy is higher for the high-temperature curve, which is in agreement with the Stoner model. The abrupt increase at higher positive energies is artificial and should not be taken into account.

The method of the normalization by the Fermi–Dirac function has the limitation that is can be applied only to energies about $\approx 5 k_B T$ above the Fermi level.[37] At $T=50$ and $T=300$ K, the validity of the method is restricted at about 21 and 120 meV above the Fermi level, respectively, while the resolution of the experiment is about 220 meV, this means that the extraction of information above the Fermi level is limited by the experimental resolution. Only the relative intensity of the two curves just below and above the Fermi level can be considered reliable.

While the above-presented valence-band spectra corrected by the Fermi–Dirac function show a temperature dependence in the intensities, we cannot rule out phonon (indirect transitions) effects as their origin instead of magnetic ones.

In order to obtain the temperature variation of the exchange splitting, we tried to measure also the Fe 3*s* at room temperature and at $T=50$ K, but we could not see any difference, as demonstrated by Fig. 10.

The magnetic splitting of the 3*s* level of iron is clearly visible and has a value of 4.3 eV (marked in the figure), typical for iron compounds. However, no change is observed as a function of the temperature, probably because the expected shift (roughly 15 meV) is too small for the experimental resolution. In order to extract the exchange splitting and its correlation with the exchange stiffness, we think a more suitable system would be one that shows stripe domains as well as a minority band less empty than FePd.

The experimental incertitudes and the lack of direct spin resolution make it impossible to extract the value of the exchange splitting. While small changes are seen in the valence-band spectra, further investigation is needed to give a conclusive picture of the changes in the density of states.

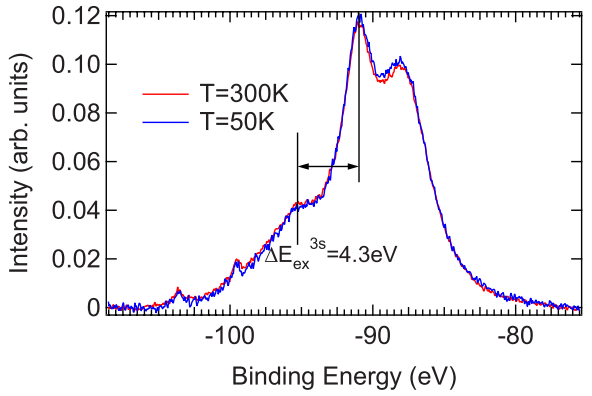

FIG. 10. (Color online) HXPES spectrum of the 3*s* core levels of iron [overlapping to the (Pd 4*s*)] at two different temperatures. To the experimental data an integral background has been subtracted and the binding energy has been referenced to the spectrum of a polycrystalline Au sample measured at the same temperature of the core-level spectra. The small peaks at 99 and 103 eV are shallow impurity levels.

For these reasons, it is not possible to relate the behavior of the mesoscopic quantity $A(T)$ with the microscopic $\Delta E_{\mathrm{ex}}(T)$.

VI. SUMMARY

To summarize our work, we have used two different approaches to determine the temperature dependence of the exchange stiffness $A(T)$, one based on the analysis of the saturation magnetization data and the other one based on an exact micromagnetic model of the nucleation point in conjunction with the experimental values of the nucleation field and domain width as a function of the temperature. We found that the experimental data behave consistently but deviate from the usual phenomenological rule used for the temperature dependence of $A(T)$. Because of this result and considerations based on the microscopic Heisenberg model, we conclude that in the examined temperature range, given the very slow temperature dependence of the exchange integral J, the magnon stiffness D must have a temperature dependence or the localized model has to be abandoned in favor of an itinerant picture. The comparison between the photoemission data and the theoretical band-structure calculations lead to the identifications of the main features of the valence band. Based on the lack of consistency of the magnetometry and scattering results compared to local-moment theories, the results favor an itinerant magnetism picture for FePd.

ACKNOWLEDGMENTS

M.M. would like to thank B. Gilles and A. Marty for supplying the sample, Y. Otani, and L. Vila for allowing the use of the magnetic force microscope, and T. Yamauchi for the assistance during the SQUID measurements. This work was partly funded by the Japanese Society for the Promotion of Science of the Ministry of Education, Culture and Sport of Japan.

APPENDIX. A, J, AND M_S IN THE HEISENBERG MODEL

We give a small derivation of the continuum limit for the exchange interaction using the Heisenberg model. It governs the behavior of compounds with magnetic moments localized on atomic lattice sites, thus it is not directly applicable to itinerant ferromagnets. The Heisenberg Hamiltonian can be written as

$$H_{\mathrm{Heis}} = -J\sum_{\langle i,j\rangle} \vec{S}_i \cdot \vec{S}_i,$$

where the sum is between the nearest neighbors of each lattice site and the spins can be considered as classical or quantum. The model gives a ferromagnetic ground state (parallel alignment of all the spins) for a positive value of J, the exchange integral, and an antiferromagnetic ground state for negative J. For simplicity we reduce the lattice to a linear chain of classical spins, thus the sum over nearest neighbors reduces to

$$H_{\mathrm{Heis}} = -2J\sum_{i=1}^{N} \vec{S}_i \cdot \vec{S}_{i+1}.$$

If an external force (like a PMA or a thermal excitation of a magnon) rotates one of the spins with respect to the others and if the spin magnitude is conserved, then we may write,

$$H_{\mathrm{Heis}} \approx -2JS^2\sum_{i=1}^{N} \cos(\theta_i - \theta_{i+1}).$$

If the angles between the spins are small, i.e., only long-wavelength deviations are allowed, then $\theta_i - \theta_{i+1} \approx \delta\theta_i$ and it is possible to approximate the cosines by a Taylor series,

$$\cos(\theta_i - \theta_{i+1}) \approx \cos(\delta\theta_i) \approx 1 - \frac{\delta\theta_i^2}{2}.$$

Then the sum in the Heisenberg Hamiltonian becomes,

$$\sum_{i=1}^{N} \cos(\delta\theta_i) \approx \sum_{i=1}^{N} \left(1 - \frac{\delta\theta_i^2}{2}\right) = E_0 + \Delta H.$$

The first term simply gives the constant energy of the system having all the spins aligned (ground state), while the second term,

$$\Delta H \approx JS^2\sum_{i=1}^{N} \delta\theta_i^2,$$

gives the energy necessary to "produce" the deviation from the uniformly magnetized state. The small variable θ_i can be regarded as the spin magnitude perpendicular to the main component S and can thus be renamed $\hat{m}_i$. Assuming only long-wavelength deviations allows to approximate $\hat{m}_i$ to a continuous field, which is a function of a coordinate $\vec{r}$ instead of it being a discrete variable on a lattice. Consequently, the sum over the lattice sites becomes an integral over the new variable $\vec{r}$,

$$\Delta H \approx H_{\mathrm{exc}} = JM_S^2 \int \left[\frac{dm(r)}{dr}\right]^2 dr.$$

Thus, from the microscopic Heisenberg Hamiltonian, the

continuum limit has been derived for classical spins on a linear chain in the approximation of long-wavelength deviations from the saturated state. The generalization to higher dimensional lattices and to three-dimensional spins just introduces some prefactors due to the different coordination number and changes the total derivative into a gradient. S, the spin magnitude, has been renamed M_S, the saturation magnetization of the film. The factor in front of the integral is exactly the exchange stiffness A, which can be now linked to the saturation magnetization and to the exchange integral,

$$A = JM_S^2. \tag{A1}$$

The exchange is one of the terms entering the energy balance of a magnetic system in the continuum limit and it has been demonstrated to be applicable to the analysis of magnetic domains of micro and nanostructures of a very wide class of materials[5,23] The relation between A, J, and M_S is very important since it establishes a link between the microscopic and mesoscopic quantities, but as a limitation it is strictly valid only for localized magnetic moments.

[1] V. Gehanno, Y. Samson, A. Marty, B. Gilles, and A. Chamberod, J. Magn. Magn. Mater. **172**, 26 (1997).

[2] V. Gehanno, A. Marty, B. Gilles, and Y. Samson, Phys. Rev. B **55**, 12552 (1997).

[3] C. Herring and C. Kittel, Phys. Rev. **81**, 869 (1951).

[4] N. W. Ashcroft and N. D. Mermin, *Solid State Physics* (Brooks-Cole, Belmont, MA, 1976).

[5] H. Kronmuller and M. Fahnie, *Micromagnetism and the Microstructure of Ferromagnetic Solids* (Cambridge University Press, Cambridge, 2003).

[6] G. Asti, M. Ghidini, M. Mulazzi, R. Pellicelli, M. Solzi, K. Chesnel, and A. Marty, Phys. Rev. B **76**, 094414 (2007).

[7] S. W. Lovesey and S. P. Collins, *X-ray Scattering and Absorption by Magnetic Materials* (Oxford University Press, New York, 1996).

[8] J. P. Hannon, G. T. Trammell, M. Blume, and D. Gibbs, Phys. Rev. Lett. **61**, 1245 (1988).

[9] M. Blume, J. Appl. Phys. **57**, 3615 (1985).

[10] H. A. Dürr, E. Dudzik, S. S. Dhesi, J. B. Goedkoop, G. van der Laan, M. Belakhovsky, C. Mocuta, A. Marty, and Y. Samson, Science **284**, 2166 (1999).

[11] E. Dudzik, S. S. Dhesi, H. A. Dürr, S. P. Collins, M. D. Roper, G. van der Laan, K. Chesnel, M. Belakhovsky, A. Marty, and Y. Samson, Phys. Rev. B **62**, 5779 (2000).

[12] M. Mulazzi, K. Chesnel, A. Marty, G. Asti, M. Ghidini, M. Solzi, M. Belakhovsky, N. Jaouen, J. M. Tonnerre, and F. Sirotti, J. Magn. Magn. Mater. **272-276**, e895 (2004).

[13] M. Sacchi, F. Offi, P. Torelli, A. Fondacaro, C. Spezzani, M. Cautero, G. Cautero, S. Huotari, M. Grioni, R. Delaunay, M. Fabrizioli, G. Vankó, G. Monaco, G. Paolicelli, G. Stefani, and G. Panaccione, Phys. Rev. B **71**, 155117 (2005).

[14] Y. Takata, in *Very High Resolution Photoelectron Spectroscopy*, Lecture Notes in Physics Vol. 715, edited by S. Hüfner (Springer, New York, 2007), p. 315.

[15] D. Garcia, R. Casero, M. Vazquez, and A. Hernando, Phys. Rev. B **63**, 104421 (2001).

[16] I. Galanakis, S. Ostanin, M. Alouani, H. Dreyssé, and J. M. Wills, Phys. Rev. B **61**, 599 (2000).

[17] S. S. A. Razee, J. B. Staunton, D. D. Johnson, B. Ginatempo, and E. Bruno, J. Phys.: Condens. Matter **13**, 8153 (2001).

[18] G. Panaccione, M. Altarelli, A. Fondacaro, A. Georges, S. Huotari, P. Lacovig, A. Lichtenstein, P. Metcalf, G. Monaco, F. Offi, L. Paolasini, A. Poteryaev, M. Sacchi, and O. Tjernberg, Phys. Rev. Lett. **97**, 116401 (2006).

[19] A. Chainani, T. Yokoya, Y. Takata, K. Tamasaku, M. Taguchi, T. Shimojima, N. Kamakura, K. Horiba, S. Tsuda, S. Shin, D. Miwa, Y. Nishino, T. Ishikawa, M. Yabashi, K. Kobayashi, H. Namatame, M. Taniguchi, K. Takada, T. Sasaki, H. Sakurai, and E. Takayama-Muromachi, Phys. Rev. B **69** 180508(R) (2004).

[20] G. Panaccione, G. Cautero, M. Cautero, A. Fondacaro, M. Grioni, P. Lacovig, G. Monaco, F. Offi, G. Paolicelli, M. Sacchi, N. Stojić, G. Stefani, R. Tommasini, and P. Torelli, J. Phys.: Condens. Matter **17**, 2671 (2005).

[21] W. F. Brown, Phys. Rev. **124**, 1348 (1961).

[22] M. W. Muller, Phys. Rev. **122**, 1485 (1961).

[23] A. Hubert and R. Schaefer, *Magnetic Domains* (Springer, New York, 1998).

[24] C. Kittel, Phys. Rev. **70**, 965 (1946).

[25] L. Landau and E. Lifshitz, Phys. Z. Sowjetunion **8**, 153 (1935).

[26] M. D. Kuz'min, Phys. Rev. Lett. **94**, 107204 (2005).

[27] F. J. Dyson, Phys. Rev. **102**, 1230 (1956).

[28] S. Foner and E. D. Thomson, J. Appl. Phys. **30**, 229S (1959).

[29] M. H. Seavey and P. E. Tannenwald, J. Appl. Phys. **30**, 227S (1959).

[30] P. Talagala, P. S. Fodor, D. Haddad, R. Naik, L. E. Wenger, P. P. Vaishnava, and V. M. Naik, Phys. Rev. B **66**, 144426 (2002).

[31] J. Weissmuller, R. D. McMichael, A. Michels, and R. D. Schulls, J. Res. Natl. Inst. Stand. Technol. **104**, 261 (1999).

[32] M. D. Kuz'min, M. Richter, and A. N. Yaresko, Phys. Rev. B **73**, 100401(R) (2006).

[33] P. Mohn, *Magnetism in the Solid State: An Introduction*, Springer Series in Solid-State Sciences (Springer, New York, 2005).

[34] J. Kübler, *Theory of Itinerant Electron Magnetism*, International Series of Monographs on Physics No. 106 (Oxford University Press, Oxford, 2000).

[35] C. Kittel, *Quantum Theory of Solids*, 2nd ed. (Wiley, New York, 1987).

[36] D. E. Eastman, F. J. Himpsel, and J. A. Knapp, Phys. Rev. Lett. **40**, 1514 (1978).

[37] T. Greber, T. J. Kreutz, and J. Osterwalder, Phys. Rev. Lett. **79**, 4465 (1997).